

Relativistic suppression of Auger recombination in Weyl semimetals

A. N. Afanasiev,^{1,2,*} A. A. Greshnov,^{1,2} and D. Svintsov²

¹*Ioffe Institute, St.Petersburg 194021, Russia*

²*Moscow Institute of Physics and Technology, Dolgoprudny 141700, Russia*

(Dated: December 15, 2024)

Auger recombination (AR) being electron-hole annihilation with energy-momentum transfer to another carrier is believed to speed up in materials with small band gap. We theoretically show that this rule is violated in gapless three-dimensional materials with ultra-relativistic electron-hole dispersion, Weyl semimetals (WSM). Namely, AR is prohibited by energy-momentum conservation laws in *prototypical* WSM with a single Weyl node, even in the presence of anisotropy and tilt. In *real* multi-node WSM, the geometric dissimilarity of nodal dispersions enables weak *inter-node* AR, which is further suppressed by strong screening due to large number of nodes. While partial AR rates between the nodes of the same node group are mutually equal, the inter-group processes are non-reciprocal, so that one of groups is *geometrically protected* from AR. Our calculations show that geometrical protection can help prolonging AR lifetime by the two orders of magnitude, up to the level of nanoseconds.

Introduction.— The latest years of condensed matter physics are marked by an intense search for solid-state realizations of exotic fundamental particles [1–3]. The unique electronic properties of graphene [4], Weyl [5–9], and Dirac [10] semimetals enabled the tabletop observation of Klein tunneling [11], supercritical atomic collapse [12], axial [13] and axial-gravitational [14] anomalies. In this strive for high-energy physics *enabled* by electronic properties of novel materials, less attention is paid to the effects *prohibited* by these properties. Such negatory search still can be fruitful. In particular, suppression of electron scattering, relaxation, and recombination in solids would enable the observation of new phases of ultra-clean matter, not to say about ultrafast electronic and photonic devices.

In this Letter, we show that quasi-relativistic dispersion of fermions in recently discovered Weyl semimetals (WSM) strongly suppresses the process of electron-hole recombination with energy-momentum transfer to another carrier, known as Auger recombination (AR). The AR is among key obstacles toward the realization of non-equilibrium phases of electron-hole liquid [15], excitonic insulator [16], as well as coherent phenomena of super-radiance [17] and photon-induced Rabi splitting [18]. In addition, AR is the primary "killer" of population inversion and optical gain in narrow-gap semiconductor lasers [19, 20] hindering their promotion into terahertz range. There were numerous attempts to suppress AR, invoking strain-engineering of band structure [21], modification of wave function profiles [22], and exchange effects upon scattering [23]. However, there has been no material with "natural" AR suppression as it occurs in WSM.

We further elaborate the incompleteness of analogy between relativistic electrons and Weyl fermions, and reveal its consequences for AR. In real WSM, there exist multiple Weyl nodes located at *low-symmetry* points of the Brillouin zone (Fig. 1), which can be attributed to one or

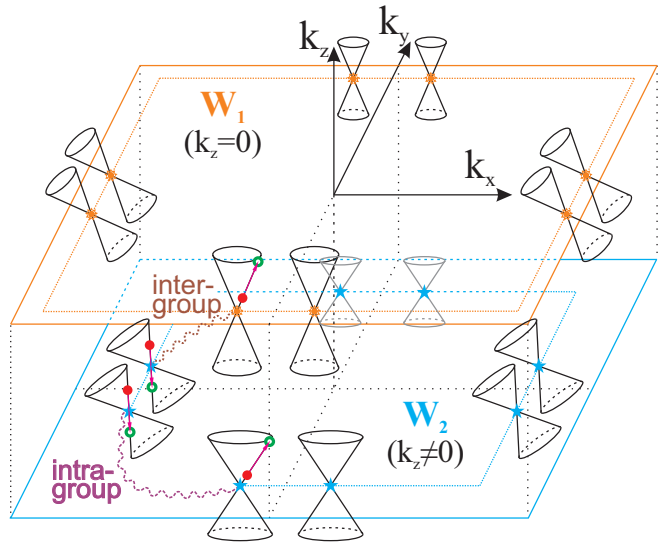


FIG. 1. Schematic structure of the Weyl nodes and inter-node AR by the example of C_{4v} point symmetry with two groups of the nodes, known as W_1 and W_2 in TaAs family of WSM. Wavy lines show the two types of the Auger processes involving two nodes of the same group or the nodes of different groups. In the latter case, the interband transition occurs in W_1 and the intraband one – in W_2 (or vice versa).

several node groups, such as in TaAs family, where the groups are known as W_1 and W_2 . As a result, the real carrier energy spectrum acquires anisotropy [24–26] and tilt. We show that it is the dissimilarity of energy spectra at different nodes that enables weak *inter-node* recombination, while the *intra-node* AR remains prohibited. The importance of a similar inter-valley AR was noted for lead salts [27], however, strong suppression of intra-valley process was not realized. Adapting Ziep-Mocker approach [28] to calculation of AR rate in WSM, we study the relaxation dynamics of interband population inversion in various regimes and show that the lifetimes

can achieve the level of 10^{-8} s thanks to geometrical protection, large number of Weyl nodes and screening.

AR in prototypical WSM.— The suppression of AR in WSM is tightly linked to the impossibility of impact ionization of Dirac vacuum by high-energy electrons. Indeed, an electron with energy-momentum relation $E^2 = (mv_0^2)^2 + (kv_0)^2$ cannot emit electron-positron pairs due to non-equal energies of initial (mv_0^2) and final states ($\geq 3mv_0^2$) in the center-of-mass system.

As the mass gap tends to zero and dispersions to the *ultra-relativistic* form, $E(\mathbf{k}) \propto k$, the situation becomes pathological. Momentum conservation for Auger process reads $\mathbf{k}_{e1} + \mathbf{k}_{h1} + \mathbf{k}_{e2} = \mathbf{k}'_{e2}$, where \mathbf{k}_{e1} and \mathbf{k}_{h1} are the momenta of recombining electron and hole (condensed matter counterpart of positron), \mathbf{k}_{e2} and \mathbf{k}'_{e2} are the initial and final momenta of 'hot' electron. The energy conservation implies $k_{e1} + k_{h1} + k_{e2} = k'_{e2}$, and renders all four momenta collinear. The phase space for collinear collisions vanishes. However, the interaction strength between collinear carriers diverges as their unidirectional motion with equal velocities implies infinite interaction time. This fact is known as collinear scattering anomaly [29], and the resulting AR probability of the form $0 \times \infty$ was shown to be finite in two dimensions [30–32].

To put the solution of this problem in three dimensions on a solid ground, we use a transparent yet not widely adopted relation [28] between AR and imaginary parts of inter- and intraband polarizations, $\text{Im}\Pi_{-+}$ and $\text{Im}\Pi_{ss}$ (here $s = \pm 1$ is the index of conduction and valence bands). The AR rate in this formalism involves the product of electron-hole annihilation probability characterized by $\text{Im}\Pi_{-+}$, the squared amplitude of virtual photon propagation, and the probability of interband photon absorption $\text{Im}\Pi_{ss}$. The formal expression for the rate of AR with energy transferred to the s -th band, $\mathcal{R}^{(s)}$, reads

$$\mathcal{R}^{(s)} = 4 \sum_{\mathbf{q}\omega} \text{Im}\Pi_{-+}(\omega, \mathbf{q}) \frac{|V_0(\mathbf{q})|^2}{|\epsilon(\omega, \mathbf{q})|^2} \text{Im}\Pi_{ss}(\omega, \mathbf{q}) \times [n_B(\omega - \Delta\mu_{eh}) - n_B(\omega)], \quad (1)$$

where $V_0(\mathbf{q}) = 4\pi e^2/q^2$ is the Fourier transform of Coulomb interaction, $\epsilon(\omega, \mathbf{q})$ is the dielectric function of WSM, $n_B(\omega) = [e^{\omega/T} - 1]^{-1}$ is the Bose distribution, and $\Delta\mu_{eh} = \mu_e - \mu_h$ is the difference of electron and hole quasi-Fermi levels [33]. Summation in (1) is performed over all possible frequencies ω and wave vectors \mathbf{q} of virtual photons, $\sum_{\mathbf{q}\omega} \equiv (2\pi)^{-4} \int d^3\mathbf{q} d\omega$.

Since the AR involves both inter- and intraband electron transitions, the domains of non-zero $\text{Im}\Pi_{-+}$ and $\text{Im}\Pi_{ss}$ should intersect in (ω, \mathbf{q}) 4-space. For prototypical WSM, these functions have well-defined boundaries:

$$\text{Im}\Pi_{-+}^{(0)} = F_{-+}(\omega, \mathbf{q})\theta(\omega - v_0 q), \quad (2)$$

$$\text{Im}\Pi_{ss}^{(0)} = F_{ss}(\omega, \mathbf{q})\theta(v_0 q - |\omega|), \quad (3)$$

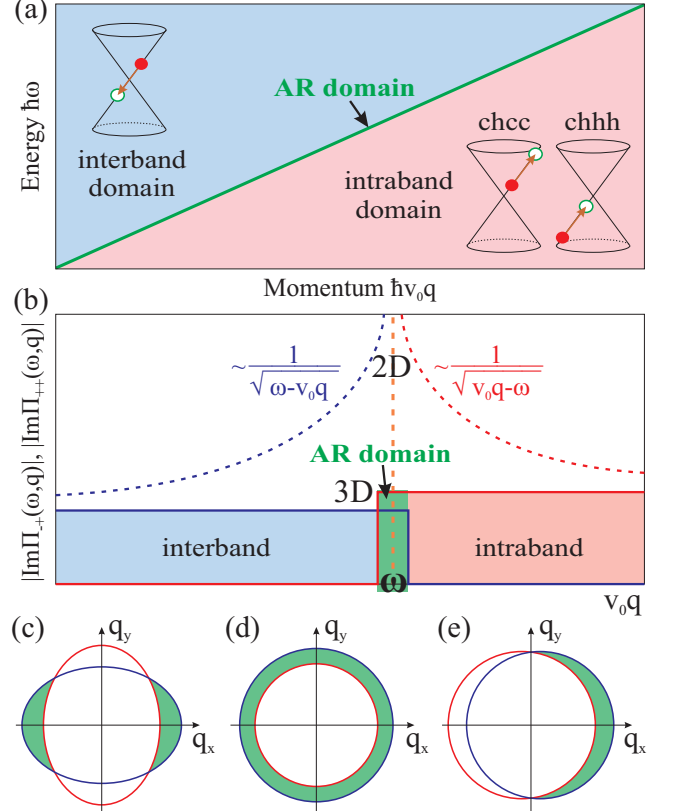


FIG. 2. Strong suppression of AR in WSM explained in terms of overlap between intra- and interband excitations (a) The domains of interband ($\text{Im}\Pi_{-+} \neq 0$) and intraband ($\text{Im}\Pi_{ss} \neq 0$) excitations are located on different sides of $\omega = v_0 q$ line in prototypical WSM. (b) Behaviour of inter- and intraband polarizations in the vicinity of borderline is smooth in three dimensions, in contrast to divergent one for the two-dimensional case. (c) (d) (e) Overlapping of the interband and intraband domains in the \mathbf{q} -phase space at fixed frequency ω (q_z is omitted for simplicity) in the cases of anisotropy (c), velocity difference (d) and tilt (e).

where $\theta(x)$ is the unit step function and $F_{ss'}(\omega, q)$ are smooth functions (the expressions are given in Supplemental Material Sec.I). The above equations imply that interband virtual photon emission is bound inside the "excitation cone", $\omega \geq v_0 q$, while intraband absorption is possible only outside of it, $\omega \leq v_0 q$, as shown in Fig. 2(a). Integration of smooth functions in (1) over the region of zero measure results in zero value of $\mathcal{R}^{(s)}$ (see Fig. 2(b)). It contrasts to the two-dimensional case (upper curves in Fig. 2(b)) where $F_{ss'}(\omega, q)$ possess square-root singularities at $\omega = v_0 q$, which resulted in finite AR rate [34,31].

AR in real WSM.— To study AR in materials with general anisotropic Weyl velocity tensor \hat{v}_n and tilt velocity \mathbf{u}_n (which are specific to the Weyl node group, W_n), we introduce the Hamiltonian

$$H_n(\mathbf{k}) = \mathbf{w}_n(\mathbf{k})\boldsymbol{\sigma} + w_n^{(t)}(\mathbf{k})\sigma_0, \quad (4)$$

where $\mathbf{w}_n(\mathbf{k}) = \hat{v}_n \mathbf{k}$ and $w_n^{(t)}(\mathbf{k}) = \mathbf{u}_n \mathbf{k}$. The eigenvalues

are

$$E_{n,s}(\mathbf{k}) = s|\mathbf{w}_n(\mathbf{k})| + w_n^{(t)}(\mathbf{k}). \quad (5)$$

Explicit form of dispersion in the nodes of the group are given by $E_{n,s}^{(i)}(\mathbf{k}) = E_{n,s}(g_n^{(i)}\mathbf{k})$, where $g_n^{(i)}$ represent operations of the point group connecting the nodes (C_{4v} for TaAs family, Fig. 1).

Linearity of the Hamiltonian (4) in momentum operators allows one to relate the polarization of anisotropic tilted i -th node $\Pi_{ss'}^{(i)}$ and the polarization of prototypical isotropic WSM $\Pi_{ss'}^{(0)}$, via a linear coordinate transform

$$\Pi_{ss'}^{(i)}(\omega, \mathbf{q}) = \Pi_{ss'}^{(0)}(\omega - \mathbf{u}_n g_n^{(i)} \mathbf{q}, v_n^{-1} \hat{v}_n g_n^{(i)} \mathbf{q}), \quad (6)$$

where $v_n = |\det \hat{v}_n|^{1/3}$ is the average Weyl velocity. This transform implies that anisotropy and tilt in dispersion translates in the respective deformation of the "excitation cones". As a result, the inter- and intra-band excitations within the same node still do not overlap in the presence of tilt and anisotropy, and intra-node AR remains forbidden.

At the same time, deformation of the Weyl cones opens up the inter-node recombination channel. Different orientation of the velocity tensors at the nodes produces overlap between interband and intraband excitations of these nodes (Fig. 2(c)). In multi-group case, the overlap appears due to different absolute values of Weyl velocity in various groups, even if velocity is isotropic (Fig. 2(d)). For both cases, finite overlap is also produced by the tilt (Fig. 2(e)).

As far as difference in dispersion of the nodes is small, the *partial* AR rate involving the nodes i and j , $R_{ij}^{(s)}$, can be factorized into the *geometric* and *statistical* parts,

$$R_{ij}^{(s)} = \mathcal{G}_{ij}^{(s)} \mathcal{S}_{ij}^{(s)}, \quad (7)$$

as proved in Supplemental Material Sec.II.

The dimensionless geometric factor \mathcal{G} originates from integration of the Coulomb amplitude $V_0(\mathbf{q})$ over the allowed wave vectors [shaded areas in Fig. 2(c-e)]. Mathematically, it is given by an integral over the solid angle of a unit vector \mathbf{e}_q ,

$$\mathcal{G}_{ij}^{(s)} = \int_{\Delta(\mathbf{e}_q) > 0} \frac{\Delta(\mathbf{e}_q) d\mathbf{e}_q}{|v_n[g_n^{(i)}]^{-1} \hat{v}_n^{-1} \mathbf{e}_q|^4}, \quad (8)$$

$$\Delta(\mathbf{e}_q) = |\hat{v}_{n'} g_{ij} \hat{v}_n^{-1} \mathbf{e}_q| - 1 - (\mathbf{u}_n - \mathbf{u}_{n'} g_{ij}) \hat{v}_n^{-1} \mathbf{e}_q, \quad (9)$$

where $g_{ij} = g_{n'}^{(j)} [g_n^{(i)}]^{-1}$, and the nodes i, j are assumed to belong to the groups $W_{n,n'}$, respectively.

Once a small difference in node dispersions is carried to \mathcal{G} , the statistical factor \mathcal{S} can be expressed via the polarization of the prototypical WSM,

$$\mathcal{S}_{ij}^{(s)} = \int \frac{\omega_q d^3 \mathbf{q}}{16\pi^5} |\tilde{V}(q)|^2 F_{-+}^{(i)}(\omega_q, q) F_{ss}^{(j)}(\omega_q, q) \mathcal{N}_B(\omega_q), \quad (10)$$

where $\tilde{V}(q) = V_0(q)/\epsilon(\omega_q, q)$, $\mathcal{N}_B(\omega) = n_B(\omega - \Delta\mu_{eh}) - n_B(\omega)$, and the frequency of virtual photon is at the edge of "excitation cone", $\omega_q = v_0 q$. The factorization allows one to evaluate and discuss the effect of a particular material band structure and that of statistics independently.

We first discuss the geometry of intra-group AR enabled by in-plane velocity anisotropy, assuming principal axis of the Weyl velocity tensor parallel to the crystallographic ones. In case of W_1 node group of TaAs, the operations of point group C_{4v} generate four Weyl velocity tensors with

$$\hat{v}^{(i)} = \text{diag}(v_x \cos \varphi_i - v_y \sin \varphi_i, v_y \cos \varphi_i + v_x \sin \varphi_i, v_z), \quad (11)$$

where $\varphi_i = 0, \pi/2, \pi, 3\pi/2$. For each pair of nodes with perpendicular dispersion surfaces, the geometric part \mathcal{G}_{xy} is given by volume between two ellipsoids in \mathbf{q} -space, as illustrated in Fig. 2(c). Explicit calculation in the limit $|v_x - v_y| \ll v_\perp = (v_x + v_y)/2$ (see Supplemental Material Sec.III) results in

$$\mathcal{G}_{xy} = \frac{|v_x - v_y|}{v_\perp} g(1 - v_z^2/v_\perp^2) \left(\frac{v_z}{v_\perp} \right)^{5/3}, \quad (12)$$

$$g(x) = \frac{\sqrt{x(1-x)} + (2x-1) \arctan \sqrt{\frac{x}{1-x}}}{(1-x)x^{3/2}}. \quad (13)$$

The AR rate does also not vanish even if node dispersions differ in tilt only. The tilt-enabled geometric factor \mathcal{G}_t is given by the volume between two shifted spheres in \mathbf{q} -space, as shown in Fig. 2(e), so that

$$\mathcal{G}_t = \frac{\pi |\mathbf{u}^{(i)} - \mathbf{u}^{(j)}|}{v_0}, \quad (14)$$

where $\mathbf{u}^{(i,j)} = \mathbf{u}_{n,n'} g_{n,n'}^{(i,j)}$, $i, j \in W_{n,n'}$, and we have assumed equal velocity tensors for different nodes.

When there exist multiple Weyl node groups, the difference in (averaged) Weyl velocities appears as a more important factor for inter-group AR than anisotropy and tilt. Neglecting the latter, the geometry factor \mathcal{G}_\odot is given by volume between two spheres in q -space, as shown in Fig. 2(d), and results in

$$\mathcal{G}_\odot = \frac{8\pi(v_2 - v_1)\theta(v_2 - v_1)}{v_1 + v_2}. \quad (15)$$

A striking feature of inter-node AR is its *non-reciprocity*, i.e. the absence of recombination in the group with fastest Weyl velocity v_* . Indeed, the virtual photon with momentum $q < \omega/v_*$ emitted upon e-h annihilation in "fast" group cannot be absorbed in "slow" nodes (while the opposite is possible). Thus, this peculiar "fast" node is *geometrically protected* from AR, provided there is no anisotropy/tilt enabling intra-group AR. Below we show that geometrical protection helps elongating the lifetimes in real WSM with enabled intra-group channel of AR up to a few nanoseconds.

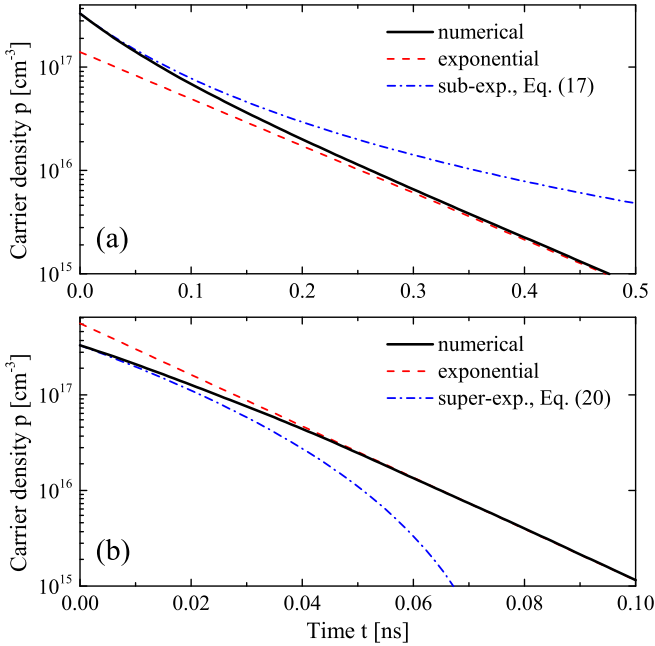


FIG. 3. Dynamics of the non-equilibrium carrier density $p(t)$ in WSM with a sole node group, intrinsic (a) and extrinsic (b). The exponential (non-degenerate) and non-exponential (degenerate) analytical limits are shown by broken lines.

Visualization of AR in WSM: temporal dynamics.—Once the interband population inversion is created in WSM, its relaxation after relatively fast intraband equilibration (due to electron-electron scattering) is governed by the interband processes. Assuming that AR lifetime in WSM is shorter than the phonon-limited lifetime [35], we consider the temporal dynamics with AR channel only,

$$\frac{dp_n}{dt} = -\mathcal{R}_n, \quad (16)$$

where $p_n(t) = n_n(t)$ are the non-equilibrium carrier densities at each node group W_n , and $\mathcal{R}_n = \sum_{j,s} \mathcal{R}_{ij}^{(s)}$ is a partial AR rate in W_n . Assuming uniform pumping at each node, we solve Eq. (16) with a given initial total non-equilibrium density p_0 distributed among the node groups according to the degeneracy factors η_n .

To account for realistic screening in WSM, we use Thomas-Fermi approximation for $\epsilon(\omega, \mathbf{q})$. The latter is proportional to the total number of nodes η , which equals 24 in TaAs family. This makes the total AR rate almost independent of the nodal degeneracy and the lifetimes – nearly proportional to η , thus enhancing them by more than an order of magnitude. For estimates, we take the average Weyl velocity $v_0 = 2.5 \cdot 10^7$ cm/s, $\varkappa = 10$, $T = 77$ K, and the geometry factors $\mathcal{G}_{1,2}$ for the intra-group and inter-group contributions as 0.1 and 0.2, respectively.

As a first example, we consider WSM with a single group of eight nodes, as expected in strained HgTe [37],

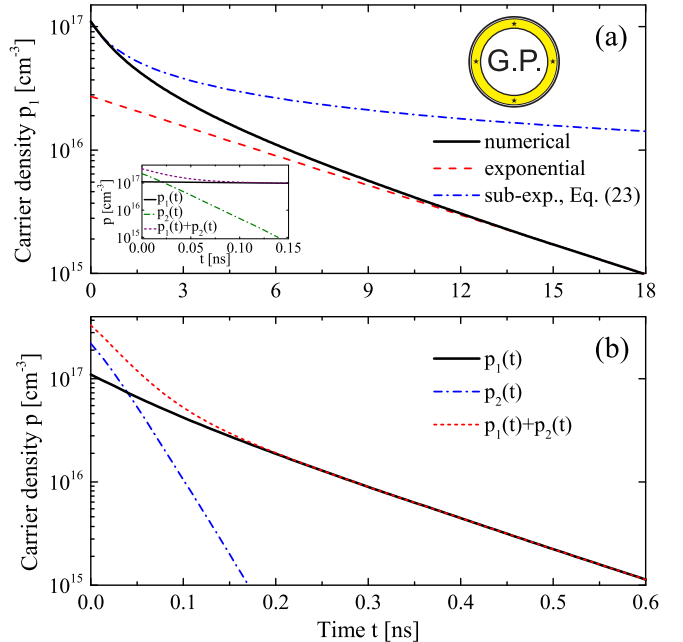


FIG. 4. Dynamics of the population inversion in WSM with 8-fold degenerate intrinsic node group W_1 and 16-fold degenerate extrinsic group W_2 with (a) and without (b) *geometrical protection* of W_1 (either $v_1 > v_2$ or $v_1 < v_2$). The inset in (a) shows fast relaxation of p_2 in contrast to long-living $p_1(t)$.

in the intrinsic limit when Fermi level in equilibrium is at the Weyl point, $\mu = 0$. Under sufficiently strong interband pumping ($p_0 = 3 \cdot 10^{17}$ cm $^{-3}$) the initial distributions of electrons and holes are symmetric and degenerate, with quasi-Fermi levels $\delta\mu = -\delta\mu_h \gg T$. In this regime, the relaxation dynamics is *sub-exponential*,

$$p(t) = \frac{p_0}{(1 + t/3\tau_0)^3}, \quad (17)$$

$$\tau_0^{-1} = C_{1d}(\alpha_\eta) \mathcal{G}_1 v_0 \eta^{-4/3} p_0^{1/3}, \quad (18)$$

where $\alpha_\eta = \eta e^2 / \varkappa v_0$ is the effective fine structure constant and $C_{1d}(\alpha_\eta)$ describes the effect of screening [36]. After initial (sub-exponential) stage of relaxation the carrier distribution turns to non-degenerate ($\delta\mu \ll T$) and the relaxation becomes exponential with

$$\tau^{-1} = C_{1n}(\alpha_\eta) \mathcal{G}_1 \eta^{-1} T. \quad (19)$$

For arbitrary position of the Fermi level, the rate of AR can be evaluated as well [36], and (16) is solved numerically, as shown in Fig. 3(a) [38].

The relaxation scenario in the extrinsic case ($\mu \gg T, \delta\mu$) is radically different. Under the same excitation of $p_0 = 3 \cdot 10^{17}$ cm $^{-3}$ the electron quasi-Fermi level is almost unaffected by pumping in WSM with residual density $n_r = 10^{18}$ cm $^{-3}$ ($\mu \approx 25$ meV), while the hole Fermi level is moved into the valence band. In this regime the

relaxation is *super-exponential*,

$$p(t) = p_0(1 - t/3\tau_0)^3, \quad (20)$$

$$\tau_0^{-1} = C_{2d}(\alpha_\eta)\mathcal{G}_1 v_0^{-1} \eta^{-2/3} \mu^2 p_0^{-1/3}. \quad (21)$$

Once density of the non-equilibrium carriers reaches the level of $\sim (T/v_0)^3$, the distribution of holes becomes non-degenerate and the relaxation is exponential with

$$\tau^{-1} = C_{2n}(\alpha_\eta)\mathcal{G}_1 \eta^{-1} T^{-1} \mu^2. \quad (22)$$

Numerical solution of Eq. (16) for the extrinsic case and the analytical limits are shown in Fig. 3(b). Comparison of the intrinsic and extrinsic cases shows that relaxation is faster in the latter by almost an order of magnitude, mainly due to the *parabolic* density of states in WSM.

The most remarkable feature of relaxation dynamics in multi-group WSM is the *geometric protection* of population inversion in nodes with large velocity. This situation is favoured by the band structure of TaAs, the first experimentally discovered WSM. It possesses the 8-fold degenerate node group W_1 , which is almost intrinsic, and the extrinsic 16-fold degenerate node group W_2 with $\mu \approx 20$ meV [1]. If all eigenvalues of the Weyl velocity tensor in W_1 are exceed those in W_2 , the inter-group channel of AR for W_1 is locked. At the same time, the intra-group channel is suppressed due to screening by large density of the resident carriers at W_2 . Therefore, one can expect extra-long lifetimes of carriers in W_1 . At the initial excitation density $p_0 = 3 \cdot 10^{17} \text{ cm}^{-3}$ the distributions at both W_1 and W_2 are degenerate, and the evolution of $p_2(t)$ is given by Eqs. (20,21) with η substituted by degeneracy of highly occupied node η_2 , while

$$p_1(t) = \frac{p_1(0)}{(1 + 5t/(3\tau_0))^{3/5}}, \quad (23)$$

$$\tau_0^{-1} = C_{3n} v_0^5 \eta_2^{-2} \eta_1^{-2/3} \mathcal{G}_1 \mu^{-4} p_1(0)^{5/3} \quad (24)$$

with $C_{3n} \approx 234$ [36]. In the non-degenerate limit of carrier distribution in W_1 and the valence band of W_2 the relaxation becomes exponential in both node groups, so the system is in multi-exponential relaxation regime. The lifetime of carriers in W_2 is given by Eq. (22) with $\eta \rightarrow \eta_2$, while for W_1

$$\tau^{-1} = C_{1n}(\beta_{\eta_2})\mathcal{G}_1 \eta_1 \eta_2^{-2} \alpha_{\eta_1}^2 \beta_{\eta_2}^{-2} T, \quad (25)$$

where $\beta_{\eta_2} = (3/\pi^2)(\mu/T)^2 \alpha_{\eta_2}$. Numerical evaluation of Eq. (16) for $p_{1,2}(t)$ (see Fig. 4(a)) illustrates that in both cases the lifetimes of *geometrically protected* carriers are by the orders of magnitude larger than those in single-group WSM (Fig. 3), the lifetimes of carriers of W_2 (the inset in Fig. 4(a)), or when the intrinsic node group is not protected ($v_1 < v_2$, Fig. 4(b)).

Conclusion. We have shown that peculiar ultra-relativistic band structure of WSM results in strong suppression of AR due to phase space restrictions imposed by

energy and momentum conservation laws. The process is allowed in multi-node WSM only, in the form of Auger scattering between Weyl nodes i and j with non-identical carrier dispersion laws $E_i(\mathbf{k}) \neq E_j(\mathbf{k})$. The nodes may be from either the same node group W_n (intra-group channel), or from different groups W_n and $W_{n'}$ (inter-group AR). In comparison to graphene, the carrier lifetimes in realistic WSM are elongated by several orders of magnitude thanks to (1) "geometrical" restrictions in phase space and (2) strong screening of Coulomb interaction proportional to the number of nodes (24 in TaAs family of WSM).

Peculiar feature of the inter-group AR is its non-reciprocity. It results in *geometrical protection* of the population inversion in the "fastest" node group W_* , where the rate of this process vanishes. In real WSM the carrier dispersion is anisotropic and tilted, so the intra-group channel is still open. However, it can be strongly suppressed if W_* is the intrinsic node group and there are enough carriers outside of it to provide intense screening. As a result, the lifetimes up to 10^{-8} s can be achieved in WSM with *geometrically protected* node group, as shown in Fig. 4(a). Fortunately, experimental and numerical studies of TaAs support band structure with one (almost) intrinsic node group, W_1 , and another extrinsic node group, W_2 , so this scenario is likely to occur in this WSM.

Our preliminary estimates show that account of dynamic screening further suppresses AR, as the real part of the screening function has a logarithmic singularity at the edge of the excitation cone [39], $\text{Re}\epsilon(q, \omega) \propto \ln|\omega - qv_0|$. This would result in an extra large log factor in carrier lifetime, order of $\ln^2 \mathcal{G}^{-1}$. All these results allow us to consider WSM as promising candidates for long-lasting non-equilibrium states and efficient coherent terahertz emission.

This work was supported by Grant No. 16-19-10557 of the Russian Science Foundation.

* afanasiev.an@mail.ru

- [1] N. P. Armitage, E. J. Mele, and A. Vishwanath, *Rev. Mod. Phys.* **90**, 015001 (2018).
- [2] G. E. Volovik, *The universe in a helium droplet*, Vol. 117 (Oxford University Press, 2003).
- [3] S. R. Elliott and M. Franz, *Rev. Mod. Phys.* **87**, 137 (2015).
- [4] K. S. Novoselov, A. K. Geim, S. Morozov, D. Jiang, M. Katsnelson, I. Grigorieva, S. Dubonos, Firsov, and AA, *Nature* **438**, 197 (2005).
- [5] B. Q. Lv, H. M. Weng, B. B. Fu, X. P. Wang, H. Miao, J. Ma, P. Richard, X. C. Huang, L. X. Zhao, G. F. Chen, Z. Fang, X. Dai, T. Qian, and H. Ding, *Phys. Rev. X* **5**, 031013 (2015).
- [6] S.-Y. Xu, I. Belopolski, N. Alidoust, M. Neupane, G. Bian, C. Zhang, R. Sankar, G. Chang, Z. Yuan, C.-

C. Lee, S.-M. Huang, H. Zheng, J. Ma, D. S. Sanchez, B. Wang, A. Bansil, F. Chou, P. P. Shibayev, H. Lin, S. Jia, and M. Z. Hasan, *Science* **349**, 613 (2015).

[7] S.-Y. Xu, I. Belopolski, D. S. Sanchez, C. Zhang, G. Chang, C. Guo, G. Bian, Z. Yuan, H. Lu, T.-R. Chang, P. P. Shibayev, M. L. Prokopovych, N. Alidoust, H. Zheng, C.-C. Lee, S.-M. Huang, R. Sankar, F. Chou, C.-H. Hsu, H.-T. Jeng, A. Bansil, T. Neupert, V. N. Strocov, H. Lin, S. Jia, and M. Z. Hasan, *Sci. Adv.* **1**, 1501092 (2015).

[8] S.-Y. Xu, N. Alidoust, I. Belopolski, Z. Yuan, G. Bian, T.-R. Chang, H. Zheng, V. N. Strocov, D. S. Sanchez, G. Chang, C. Zhang, D. Mou, Y. Wu, L. Huang, C.-C. Lee, S.-M. Huang, B. Wang, A. Bansil, H.-T. Jeng, T. Neupert, A. Kaminski, H. Lin, S. Jia, and M. Zahid Hasan, *Nat. Phys.* **11**, 748 (2015).

[9] Z. A. Devizorova and V. A. Volkov, *Phys. Rev. B* **95**, 081302 (2017).

[10] Z. K. Liu, B. Zhou, Y. Zhang, Z. J. Wang, H. M. Weng, D. Prabhakaran, S.-K. Mo, Z. X. Shen, Z. Fang, X. Dai, Z. Hussain, and Y. L. Chen, *Science* **343**, 864 (2014).

[11] N. Stander, B. Huard, and D. Goldhaber-Gordon, *Phys. Rev. Lett.* **102**, 026807 (2009).

[12] Y. Wang, D. Wong, A. V. Shytov, V. W. Brar, S. Choi, Q. Wu, H.-Z. Tsai, W. Regan, A. Zettl, R. K. Kawakami, S. G. Louie, L. S. Levitov, and M. F. Crommie, *Science* **340**, 734 (2013).

[13] C.-L. Zhang, S.-Y. Xu, I. Belopolski, Z. Yuan, Z. Lin, B. Tong, G. Bian, N. Alidoust, C.-C. Lee, S.-M. Huang, *et al.*, *Nature communications* **7**, 10735 (2016).

[14] J. Gooth, A. C. Niemann, T. Meng, A. G. Grushin, K. Landsteiner, B. Gotsmann, F. Menges, M. Schmidt, C. Shekhar, V. Süß, R. Hühne, B. Rellinghaus, C. Felser, B. Yan, and K. Nielsch, *Nature* **547**, 324 (2017).

[15] L. Keldysh, *Contemporary physics* **27**, 395 (1986).

[16] C. Triola, A. Pertsova, R. S. Markiewicz, and A. V. Balatsky, *Phys. Rev. B* **95**, 205410 (2017).

[17] T. Laurent, Y. Todorov, A. Vasanelli, A. Delteil, C. Sirtori, I. Sagnes, and G. Beaudoin, *Phys. Rev. Lett.* **115**, 187402 (2015).

[18] O. V. Kibis, *Phys. Rev. B* **81**, 165433 (2010).

[19] J. Iveland, L. Martinelli, J. Peretti, J. S. Speck, and C. Weisbuch, *Phys. Rev. Lett.* **110**, 177406 (2013).

[20] S. V. Morozov, V. V. Rumyantsev, M. A. Fadeev, M. S. Zholudev, K. E. Kudryavtsev, A. V. Antonov, A. M. Kadykov, A. A. Dubinov, N. N. Mikhailov, S. A. Dvoretsky, and V. I. Gavrilenko, *Applied Physics Letters* **111**, 192101 (2017).

[21] C. Pidgeon, C. Ciesla, and B. Murdin, *Progress in Quantum Electronics* **21**, 361 (1997).

[22] G. E. Cragg and A. L. Efros, *Nano Letters* **10**, 313 (2010), pMID: 20017564.

[23] M. Nawrocki, Y. G. Rubo, J. P. Lascaray, and D. Coquillat, *Phys. Rev. B* **52**, R2241 (1995).

[24] F. Arnold, C. Shekhar, S.-C. Wu, Y. Sun, R. D. dos Reis, N. Kumar, M. Naumann, M. O. Ajeesh, M. Schmidt, A. G. Grushin, J. H. Bardarson, M. Baenitz, D. Sokolov, H. Borrman, M. Nicklas, C. Felser, E. Hassinger, and B. Yan, *Nature Comm.* **7**, 11615 (2016).

[25] J. Hu, J. Y. Liu, D. Graf, S. M. A. Radmanesh, D. J. Adams, A. Chuang, Y. Wang, I. Chiorescu, J. Wei, L. Spinu, and Z. Q. Mao, *Sci. Rep.* **6**, 18674 (2016).

[26] J. Klotz, S.-C. Wu, C. Shekhar, Y. Sun, M. Schmidt, M. Nicklas, M. Baenitz, M. Uhlarz, J. Wosnitza, C. Felser, and B. Yan, *Phys. Rev. B* **93**, 121105 (2016).

[27] P. R. Emtage, *Journal of Applied Physics* **47**, 2565 (1976).

[28] O. Ziep and M. Mocker, *Phys. Status Solidi B* **98**, 133 (1980).

[29] L. Fritz, J. Schmalian, M. Müller, and S. Sachdev, *Phys. Rev. B* **78**, 085416 (2008).

[30] T. Winzer and E. Malic, *Phys. Rev. B* **85**, 241404 (2012).

[31] A. Tomadin, D. Brida, G. Cerullo, A. C. Ferrari, and M. Polini, *Phys. Rev. B* **88**, 035430 (2013).

[32] G. Alymov, V. Vyurkov, V. Ryzhii, A. Satou, and D. Svitsov, *Phys. Rev. B* **97**, 205411 (2018).

[33] We note that actually Eq. (1) incorporates both Auger recombination and generation processes, therefore it vanishes in equilibrium and is an exclusive term in the r.h.s. of kinetic equation from Auger.

[34] F. Rana, *Phys. Rev. B* **76**, 155431 (2007).

[35] S. Huang, M. Sanderson, J. Tian, Q. Chen, F. Wang, and C. Zhang, *Journal of Physics D: Applied Physics* **51**, 015101 (2018).

[36] See Supplemental Material Sec.IV.

[37] J. Ruan, S.-K. Jian, H. Yao, H. Zhang, S.-C. Zhang, and D. Xing, *Nature Communications* **7**, 11136 (2016).

[38] The lifetimes used for plotting the analytical curves on Figs. 3 and 4 were taken in more refined approximations than given in text, for better agreement with numericals.

[39] M. Lv and S.-C. Zhang, *International Journal of Modern Physics B* **27**, 1350177 (2013).

SUPPORTING INFORMATION TO "RELATIVISTIC SUPPRESSION OF AUGER RECOMBINATION IN WEYL SEMIMETALS"

IMAGINARY PARTS OF POLARIZABILITIES IN WEYL SEMIMETALS

The RPA polarizability due to electron transitions between s -th and s' -th bands is given by [39]

$$\Pi_{ss'}(\omega, \mathbf{q}) = \frac{\eta}{V} \sum_{\mathbf{k}} \frac{f_s(E_{s\mathbf{k}}) - f_{s'}(E_{s'\mathbf{k}'})}{\omega + E_{s\mathbf{k}} - E_{s'\mathbf{k}'} + i0} \mathcal{I}_{ss'}(\mathbf{k}, \mathbf{k}'), \quad (S1)$$

where $s, s' = \pm 1$, η is the number of Weyl points of a given type, $\mathbf{k}' = \mathbf{k} + \mathbf{q}$, $f_s(E_{s\mathbf{k}})$ is the Fermi function with quasi-Fermi energy μ_s , $\mathcal{I}_{ss'}(\mathbf{k}, \mathbf{k}')$ is the squared overlap integral between states $\{s\mathbf{k}\}$ and $\{s'\mathbf{k}'\}$. The imaginary part

of polarizability is obtained from (S1) with Sokhotski theorem

$$\text{Im}\Pi_{ss'}(\omega, \mathbf{q}) = -\eta\pi \int \frac{d\mathbf{k}}{(2\pi)^3} \mathcal{I}_{ss'}(\mathbf{k}, \mathbf{k}') [f_s(E_{s\mathbf{k}}) - f_{s'}(E_{s'\mathbf{k}'})] \delta(\omega + E_{s\mathbf{k}} - E_{s'\mathbf{k}'}) . \quad (\text{S2})$$

The spectrum of a prototypical WSM is $E_{s\mathbf{k}} = sv_0k$, while the squared overlap integral takes on the form

$$\mathcal{I}_{ss'}(\mathbf{k}, \mathbf{k}') = \frac{1}{2} \left(1 + ss' \frac{\mathbf{k}\mathbf{k}'}{kk'} \right) . \quad (\text{S3})$$

For brevity, we set from now on the Weyl velocity to unity, $v_0 \equiv 1$. This allows us to transform (S2):

$$\begin{aligned} \text{Im}\Pi_{ss'}^{(0)}(\omega, \mathbf{q}) = -\frac{\eta ss'}{16\pi q} \int_0^{+\infty} dk \int_{|k-q|}^{k+q} dk' \delta(\omega + sk - s'k') \times \\ \times [(sk + s'k')^2 - q^2] [f_s(sk) - f_{s'}(s'k')] . \end{aligned} \quad (\text{S4})$$

The latter form was achieved by passing from integration over the spherical angles to the integration over the modulus of $k' = |\mathbf{k} + \mathbf{q}|$. Considering separately the regions $k > q$ and $k < q$ and performing the change of variable $k = (\omega + qx)/2$, we obtain the final expressions for inter- and intraband parts of WSM polarizability ($\omega_{\mathbf{q}} = v_0q$):

$$\text{Im}\Pi_{ss}^{(0)}(\omega, q) = \Theta(\omega_{\mathbf{q}} - \omega) F_{ss}(\omega, q) \quad (\text{S5})$$

$$F_{ss}(\omega, q) = -s \frac{\omega_{\mathbf{q}}^2}{32\pi v_0^3} \int_1^{+\infty} dx (x^2 - 1) \left[f_s \left(s \frac{\omega_{\mathbf{q}}x - \omega}{2} \right) - f_s \left(s \frac{\omega_{\mathbf{q}}x + \omega}{2} \right) \right] \quad (\text{S6})$$

$$\text{Im}\Pi_{-s,s}^{(0)}(\omega, q) = \Theta(s\omega - \omega_{\mathbf{q}}) F_{-ss}(\omega, q) \quad (\text{S7})$$

$$F_{-s,s}(\omega, q) = -\frac{\omega_q^2}{32\pi v_0^3} \int_{-1}^1 dx (1 - x^2) \left[f_{-s} \left(-s \frac{\omega_{\mathbf{q}}x + \omega}{2} \right) - f_s \left(s \frac{\omega - \omega_{\mathbf{q}}x}{2} \right) \right] \quad (\text{S8})$$

AUGER RECOMBINATION RATE FACTORIZATION

The general expression for AR rate between Weyl nodes i and j belonging to the groups W_n and $W_{n'}$ has the form

$$\mathcal{R}_{ij}^{(s)} = 4 \sum_{\mathbf{q}\omega} \text{Im}\Pi_{-+}^{(i)}(\omega, \mathbf{q}) \frac{|V_0(q)|^2}{|\epsilon(\omega, \mathbf{q})|^2} \text{Im}\Pi_{ss}^{(j)}(\omega, \mathbf{q}) \mathcal{N}_B(\omega), \quad (\text{S9})$$

where $\mathcal{N}_B(\omega) = n_B(\omega - \Delta\mu_{eh}) - n_B(\omega)$ and $\Pi_{-+}^{(i)}(\omega, \mathbf{q}) = \Pi_{-1,1}^{(i)}(\omega, \mathbf{q})$. Using Eq. (6) of the main text and expressions (S5)-(S8), we can re-write the imaginary parts of polarizabilities $\Pi_{ss'}^{(i,j)}$ for anisotropic Weyl nodes as

$$\text{Im}\Pi_{-+}^{(i)}(\omega, \mathbf{q}) = \Theta(\omega - \tilde{\omega}_i(\mathbf{q})) F_{-+}^{(0)}(\omega_i(\mathbf{q}), q_i) \quad (\text{S10})$$

$$\text{Im}\Pi_{ss}^{(j)}(\omega, \mathbf{q}) = \Theta(\tilde{\omega}_j(\mathbf{q}) - \omega) F_{ss}^{(0)}(\omega_j(\mathbf{q}), q_j) \quad (\text{S11})$$

$$\omega_i(\mathbf{q}) = \omega - \mathbf{u}_n g_n^{(i)} \mathbf{q} \quad (\text{S12})$$

$$\tilde{\omega}_i(\mathbf{q}) = |\hat{v}_n g_n^{(i)} \mathbf{q}| + \mathbf{u}_n g_n^{(i)} \mathbf{q} \quad (\text{S13})$$

$$\mathbf{q}_i = v_n^{-1} \hat{v}_n g_n^{(i)} \mathbf{q}, \quad (\text{S14})$$

The velocity of prototypical WSM is taken as average velocity, $v_{n,n'} = \sqrt[3]{|\det \hat{v}_{n,n'}|}$, while $\omega_j(\mathbf{q}), \tilde{\omega}_j(\mathbf{q}), \mathbf{q}_j$ are the same as (S12)-(S14) with replacements $i \rightarrow j, n \rightarrow n'$. We note that deriving these expressions in the presence of tilt, $\mathbf{u}_n \neq 0$, we can neglect the tilt in the arguments of distribution functions and, hence, in Eqs. (S6) and (S8). This is justified by the relatives smallness of tilt in type-I WSM, $|\mathbf{u}_n| \ll \|\hat{v}_n\|$. As a result, the expression for ARR is transformed into

$$\mathcal{R}_{ij}^{(s)} = 4 \int \Theta(\tilde{\omega}_j(\mathbf{q}) - \tilde{\omega}_i(\mathbf{q})) \frac{d\mathbf{q}}{(2\pi)^3} \int_{\tilde{\omega}_i(\mathbf{q})}^{\tilde{\omega}_j(\mathbf{q})} \frac{d\omega}{2\pi} F_{-+}^{(0)}(\omega_i(\mathbf{q}), q_i) \frac{|V_0(q)|^2}{|\epsilon(\omega, \mathbf{q})|^2} F_{ss}^{(0)}(\omega_j(\mathbf{q}), q_j) \mathcal{N}_B(\omega), \quad (\text{S15})$$

To proceed further, we perform the integration variable change $\mathbf{q} \rightarrow \mathbf{q}_i$ which transforms the dispersion term, associated with the Weyl velocity, into isotropic one $|\hat{v}_i \mathbf{q}| = v_n |\mathbf{q}_i|$. Henceforth, we rename the new variable as \mathbf{q} , and the expression for the ARR takes the form

$$\mathcal{R}_{ij}^{(s)} = 4 \int_0^{+\infty} \frac{q^2 dq}{(2\pi)^4} \int \frac{\Theta(\Delta(\mathbf{e}_q)) d\mathbf{e}_q}{|v_n[g_n^{(i)}]^{-1} \hat{v}_n^{-1} \mathbf{e}_q|^4} \int_{\tilde{\omega}_i(\mathbf{Q})}^{\tilde{\omega}_j(\mathbf{Q})} F_{-+}^{(0)}(\omega_i(\mathbf{Q}), q) \frac{|V_0(q)|^2}{|\epsilon(\omega, \mathbf{Q})|^2} F_{ss}^{(0)}(\omega_j(\mathbf{Q}), q_{ij}) \mathcal{N}_B(\omega), \quad (\text{S16})$$

where $\mathbf{Q} = v_n[g_n^{(i)}]^{-1} \hat{v}_n^{-1} \mathbf{q}$, $q_{ij} = |(v_n/v_{n'}) \hat{v}_{n'} g_{ij} \hat{v}_n^{-1} \mathbf{q}|$, $g_{ij} = g_{n'}^{(j)} [g_n^{(i)}]^{-1}$. In (S16) we have factorized \mathbf{q} -integration and “bare” Coulomb interaction into radial $q = |\mathbf{q}|$ and angular $\mathbf{e}_q = \mathbf{q}/q$ parts

$$|V_0(\mathbf{Q})|^2 = \frac{|V_0(q)|^2}{|v_n[g_n^{(i)}]^{-1} \hat{v}_n^{-1} \mathbf{e}_q|^4}. \quad (\text{S17})$$

The domain of the allowed (ω, \mathbf{e}_q) is determined by

$$\Delta(\mathbf{e}_q) = \frac{\tilde{\omega}_j(\mathbf{Q}) - \tilde{\omega}_i(\mathbf{Q})}{v_n q} = |\hat{v}_{n'} g_{ij} \hat{v}_n^{-1} \mathbf{e}_q| - 1 - (\mathbf{u}_n - \mathbf{u}_{n'} g_{ij}) \hat{v}_n^{-1} \mathbf{e}_q \quad (\text{S18})$$

$$\Delta(\mathbf{e}_q) > 0, \quad (\text{S19})$$

where $\Delta(\mathbf{e}_q)$ is its thickness over ω in the units of $\omega_q = v_n q$, being nonzero due to the dissimilarity in the nodes’ i and j dispersion.

We limit ourselves to the case when this difference is small. Then, due to $\Delta(\mathbf{e}_q) \ll 1$, $\omega_{i,j}(\mathbf{Q}) \approx \omega_q$, $v_{n'} \approx v_n = v_0$. Since the dependence of the integrand in (S16) on ω is determined by the smooth behaviour of the distribution functions, in (S16) we can neglect the difference between $\omega_{i,j}(\mathbf{Q})$ and ω_q everywhere, except the variation range of ω

$$\mathcal{R}_{ij}^{(s)} = 4 \int_0^{+\infty} \frac{q^2 dq}{(2\pi)^4} \int_{\Delta(\mathbf{e}_q) > 0} \frac{\Delta(\mathbf{e}_q) d\mathbf{e}_q}{|v_n[g_n^{(i)}]^{-1} \hat{v}_n^{-1} \mathbf{e}_q|^4} F_{-+}^{(0)}(\omega_q, q) \frac{|V_0(q)|^2}{|\epsilon(\omega_q, \mathbf{Q})|^2} F_{ss}^{(0)}(\omega_q, q_{ij}) \mathcal{N}_B(\omega). \quad (\text{S20})$$

We note, that the given expression for ARR is valid only if the dielectric function has no singularities in the frequency range $[\tilde{\omega}_i(\mathbf{Q}), \tilde{\omega}_j(\mathbf{Q})]$. Otherwise, the $\epsilon(\omega)$ dependence should be taken into account when calculating the integral over ω . Analogically, due to the small difference in nodes’ i and j dispersions, $q_{ij} \approx q$. Thus, integration over q and \mathbf{e}_q can be carried separately, so that $R_{ij}^{(s)}$ is factorized into the *geometric* and *statistical* parts

$$R_{ij}^{(s)} = \mathcal{G}_{ij}^{(s)} \mathcal{S}_{ij}^{(s)} \quad (\text{S21})$$

$$\mathcal{G}_{ij}^{(s)} = \int_{\Delta(\mathbf{e}_q) > 0} \frac{\Delta(\mathbf{e}_q) d\mathbf{e}_q}{|v_n[g_n^{(i)}]^{-1} \hat{v}_n^{-1} \mathbf{e}_q|^4} \quad (\text{S22})$$

$$\mathcal{S}_{ij}^{(s)} = \int \frac{\omega_q d^3 \mathbf{q}}{16\pi^5} \frac{|V_0(q)|^2}{|\epsilon(\omega_q, q)|^2} F_{-+}^{(i)}(\omega_q, q) F_{ss}^{(j)}(\omega_q, q) \mathcal{N}_B(\omega_q). \quad (\text{S23})$$

Strictly speaking, such factorization is valid only when $\epsilon(\omega, \mathbf{q}) = \kappa$. In general case, $\epsilon(\omega_q, \mathbf{Q})$ contains the combinations of q and $|v_n[g_n^{(i)}]^{-1} \hat{v}_n^{-1} \mathbf{e}_q|^2$, so that factorization becomes possible only with the dielectric function, averaged over \mathbf{e}_q directions: $\epsilon(\omega_q, q) = \langle \epsilon(\omega_q, \mathbf{Q}) \rangle_{\mathbf{e}_q}$.

GEOMETRY FACTOR

The direct evaluation of geometrical factor is most convenient if \mathcal{G}_{ij} is written directly in terms of Weyl parameters of the nodes i and j

$$\mathcal{G}_{ij} = \int_{\Delta(\mathbf{e}_q) > 0} \frac{\Delta(\mathbf{e}_q) d\mathbf{e}_q}{|v_n[\hat{v}^{(i)}]^{-1} \mathbf{e}_q|^4}, \quad (\text{S24})$$

$$\Delta(\mathbf{e}_q) = \left| \hat{v}^{(j)} [\hat{v}^{(i)}]^{-1} \mathbf{e}_q \right| - 1 - (\mathbf{u}^{(i)} - \mathbf{u}^{(j)}) [\hat{v}^{(i)}]^{-1} \mathbf{e}_q, \quad (\text{S25})$$

where $\hat{v}^{(i,j)} = \hat{v}_{n,n'} g_{n,n'}^{(i,j)}$, $\mathbf{u}^{(i,j)} = \mathbf{u}_{n,n'} g_{n,n'}^{(i,j)}$. In further calculations, we shall use both Cartesian $\mathbf{e}_q = (e_x, e_y, e_z)$ and spherical coordinates $\mathbf{e}_q = (\sin \theta \cos \varphi, \sin \theta \sin \varphi, \cos \theta)$ for the unit vector \mathbf{e}_q .

Intra-group AR enabled by in-plane velocity anisotropy

We evaluate the geometrical factor \mathcal{G}_{xy} using the pair of Weyl points with $\varphi_i = 0$ and $\varphi_j = \pi/2$ as an example. The explicit form of their velocity tensors is

$$\hat{v}^{(i)} = \hat{v}^{(xy)} = \text{diag}(v_x, v_y, v_z) \quad (\text{S26})$$

$$\hat{v}^{(j)} = \hat{v}^{(xy\perp)} = \text{diag}(-v_y, v_x, v_z). \quad (\text{S27})$$

The "anisotropy term" in the denominator of geometrical factor has the form

$$|v_n[\hat{v}^{(xy)}]^{-1}\mathbf{e}_q|^4 = (v_x v_y v_z)^{4/3} \left(\frac{\cos^2 \theta}{v_z^2} + \sin^2 \theta \left(\frac{\cos^2 \varphi}{v_x^2} + \frac{\sin^2 \varphi}{v_y^2} \right) \right)^2. \quad (\text{S28})$$

The domain of allowed (ω, \mathbf{e}_q) (in the coordinates turning the dispersion of the i -th node into isotropic one) represents the intersect of the interior of sphere and exterior of ellipsoid. The local thickness of this domain

$$\Delta(\mathbf{e}_q) = \sqrt{e_x^2 \frac{v_y^2}{v_x^2} + e_y^2 \frac{v_x^2}{v_y^2} + e_z^2 - 1}. \quad (\text{S29})$$

Introducing the eccentricity of constant energy ellipsoid in the xy -plane

$$\epsilon_{xy} = \sqrt{1 - \frac{v_x^2}{v_y^2}}, \quad (\text{S30})$$

we rewrite (S29) as

$$\Delta(\mathbf{e}_q) = \sqrt{1 - e_y^2 \epsilon_{xy}^2 + e_x^2 \frac{\epsilon_{xy}^2}{1 - \epsilon_{xy}^2}} - 1. \quad (\text{S31})$$

As mentioned before, we assume the Weyl parameters of the valleys involved to be almost identical. In particular, this implies weak anisotropy in the xy plane: $\epsilon_{xy} \ll 1$, which is equivalent to $|v_x - v_y| \ll v_\perp = (v_x + v_y)/2$. The thickness of allowed domain, in this limit, reduces to

$$\Delta(\mathbf{e}_q) = \frac{\epsilon_{xy}^2}{2} \sin^2 \theta \cos 2\varphi \quad (\text{S32})$$

$$\Delta(\mathbf{e}_q) > 0 \rightarrow -\frac{\pi}{4} < \varphi < \frac{\pi}{4}, \quad (\text{S33})$$

and will be small as far as ϵ_{xy} is small. The denominator of geometry factor, in the same limit, takes a simpler form

$$|v_n \hat{v}_{xy}^{-1} \mathbf{e}_q|^4 \approx \frac{(1 - \epsilon_z^2 \sin^2 \theta)^2}{(1 - \epsilon_z^2)^{4/3}}, \quad (\text{S34})$$

where $\epsilon_z = \sqrt{1 - (v_z/v_\perp)^2}$. Then

$$\mathcal{G}_{xy} = (1 - \epsilon_z^2) \frac{\epsilon_{xy}^2}{2} \int_{-\frac{\pi}{4}}^{\frac{\pi}{4}} \cos 2\varphi d\varphi \int_0^\pi \frac{\sin^3 \theta d\theta}{(1 - \epsilon_z^2 \sin^2 \theta)^2}. \quad (\text{S35})$$

Direct evaluation of the latter integral leads us to the final result

$$\mathcal{G}_{xy} = \frac{|v_x - v_y|}{v_\perp} g(1 - v_z^2/v_\perp^2) \left(\frac{v_z}{v_\perp} \right)^{5/3} \quad (\text{S36})$$

$$\mathcal{G}_{xy} = (1 - \epsilon_z^2)^{5/6} g(\epsilon_z^2) \frac{\epsilon_{xy}^2}{2} \quad (\text{S37})$$

$$g(x) = \frac{\sqrt{x(1-x)} + (2x-1) \arctan \sqrt{\frac{x}{1-x}}}{(1-x)x^{3/2}} \quad (\text{S38})$$

$$(\text{S39})$$

Inter-group AR

The recombination between different node groups is enabled already by the difference of absolute values of Weyl velocities. For this reason, we omit tilt and consider velocity tensor as isotropic

$$\hat{v}^{(i)} = \hat{v}^{(1)} = v_1 \delta_{lm} \quad (\text{S40})$$

$$\hat{v}^{(j)} = \hat{v}^{(2)} = v_2 \delta_{lm}, \quad (\text{S41})$$

and the process is allowed only if $v_2 > v_1$. In this recombination mechanism, no symmetry relations between nodes are required and the smallness of the domain of allowed (ω, \mathbf{q}) is guaranteed by proximity of v_2 and v_1 . Therefore

$$|v_n[\hat{v}^{(1)}]^{-1} \mathbf{e}_q|^4 = 1 \quad (\text{S42})$$

$$\Delta(\mathbf{e}_q) = 2 \frac{v_2 - v_1}{v_1 + v_2}. \quad (\text{S43})$$

Then

$$\mathcal{G}_\odot = \frac{8\pi(v_2 - v_1)\theta(v_2 - v_1)}{v_1 + v_2}. \quad (\text{S44})$$

Tilt-enabled AR

To highlight the effect of tilt-enabled AR, we omit the velocity anisotropy from consideration and take the velocity tensors of i -th and j -th nodes to be

$$\hat{v}^{(i,j)} = v_0 \delta_{lm}. \quad (\text{S45})$$

The tilt vectors of the nodes can be, however, different

$$\mathbf{u}^{(i)} = (u_x^{(i)}, u_y^{(i)}, u_z^{(i)}) \quad (\text{S46})$$

$$\mathbf{u}^{(j)} = (u_x^{(j)}, u_y^{(j)}, u_z^{(j)}). \quad (\text{S47})$$

The indices i and j can belong to different groups (W_n and $W_{n'}$) or to one group. In the latter case, the tilt vectors are related via symmetry operations. In particular, for a pair of nodes from Sec. IIIA:

$$\mathbf{u}^{(i)} = (u_x^{(i)}, u_y^{(i)}, u_z^{(i)}) \quad (\text{S48})$$

$$\mathbf{u}^{(j)} = (-u_y^{(i)}, u_x^{(i)}, u_z^{(i)}). \quad (\text{S49})$$

We note that in the case of tilt-enabled AR, the vectors $\mathbf{u}^{(j)}$ and $\mathbf{u}^{(i)}$ should not necessarily be close to each other. Indeed, the smallness of domain of allowed frequencies ω is governed by

$$\Delta(\mathbf{e}_q) = \frac{(\mathbf{u}^{(j)} - \mathbf{u}^{(i)})\mathbf{e}_q}{v_0} \quad (\text{S50})$$

and is enabled by the smallness of $\mathbf{u}^{(i,j)}$ as compared with Weyl velocity v_0 . Using the Weyl parameters from Sec. IIIA, we obtain

$$|v_n[\hat{v}^{(i)}]^{-1} \mathbf{e}_q|^4 = 1. \quad (\text{S51})$$

The expression for geometrical part takes on the form

$$\mathcal{G}_t = \int_{\mathbf{u}^{(j)}\mathbf{e}_q > \mathbf{u}^{(i)}\mathbf{e}_q} \frac{(\mathbf{u}^{(j)} - \mathbf{u}^{(i)})\mathbf{e}_q}{v_0} d\mathbf{e}_q. \quad (\text{S52})$$

To evaluate the latter, we direct the z -axis along $\mathbf{u}^{(j)} - \mathbf{u}^{(i)}$, then $(\mathbf{u}^{(j)} - \mathbf{u}^{(i)})\mathbf{e}_q = |\mathbf{u}^{(j)} - \mathbf{u}^{(i)}| \cos \theta$. The resulting expression reads

$$\mathcal{G}_t = \frac{\pi |\mathbf{u}^{(j)} - \mathbf{u}^{(i)}|}{v_0}. \quad (\text{S53})$$

STATISTICAL FACTOR AND SCREENING

In this section, we give explicit expressions for statistical factors corresponding to various initial occupations and pumping regimes and provide the particular form of distributions and dielectric functions used to calculate them.

Intra-group recombination. Sub-exponential relaxation in the intrinsic node group.

Symmetric pumping of intrinsic node leads to equal quasi-Fermi levels of electrons and holes which we denote as $\delta\mu$, $\mu_c = \delta\mu$, $\mu_v = -\delta\mu$. In the degenerate limit $\mu_c, |\mu_v| \gg T$, the distribution functions can be regarded as step-wise:

$$f_c(E) = \Theta(\delta\mu - E), \quad (\text{S54})$$

$$f_v(E) = \Theta(-\delta\mu - E). \quad (\text{S55})$$

The non-equilibrium carrier densities are related to quasi-Fermi level via

$$n = p = \frac{\eta}{6\pi^2} \frac{\delta\mu^3}{v_0^3}. \quad (\text{S56})$$

The screening function in the degenerate limit reads

$$\epsilon(0, q) = 1 + \frac{4\alpha_\eta}{\pi} \frac{\delta\mu^2}{\omega_q^2}, \quad (\text{S57})$$

where $\alpha_\eta = \frac{\eta e^2}{v_0 \hbar}$ is the effective fine structure constant which determines the strength of screening. In WSM, $\alpha_\eta \gg 1$ due to large number of nodes.

With the above assumptions, the statistical factor can be evaluated analytically:

$$\mathcal{S} = C_{1d}(\alpha_\eta) v_0 \frac{p^{4/3}}{\eta^{4/3}} \quad (\text{S58})$$

$$C_{1d}(\alpha) = \frac{\alpha^2 6^{1/3}}{4\pi^{10/3}} \left[8\alpha(\alpha + \pi) \ln \alpha - (3\pi^2 + 12\pi\alpha + 8\alpha^2) \ln \left(\alpha + \frac{\pi}{4} \right) + \pi(3\pi + 4\alpha) \ln(\pi + \alpha) + 2\sqrt{\alpha\pi^3} \arctan \left(\frac{\sqrt{\pi\alpha}}{\pi + 2\alpha} \right) - \frac{9\pi^2}{4} + 2\pi\alpha \right]. \quad (\text{S59})$$

The limiting forms of the screening function are

$$C_{1d}(\alpha) \propto \frac{3(8 \ln 2 - 3) 6^{1/3} \alpha^2}{16\pi^{4/3}} \quad (\alpha \rightarrow 0), \quad (\text{S60})$$

$$C_{1d}(\alpha) \rightarrow \frac{499}{7680} \pi^{2/3} 6^{1/3} \quad (\alpha \rightarrow \infty). \quad (\text{S61})$$

Intra-group recombination. Exponential relaxation in the intrinsic node group.

When quasi-Fermi level of pumped carriers is low $\delta\mu \ll T$, the non-equilibrium carrier density becomes a linear function of $\delta\mu$:

$$n = p = \frac{\eta}{12} \frac{T^2 \delta\mu}{v_0^3}. \quad (\text{S62})$$

The dielectric constant is governed both by thermal and non-equilibrium carriers:

$$\varepsilon_{hb}(0, q) = 1 + \frac{2\pi\alpha_\eta}{3} \frac{T^2}{\omega_q^2} \left[1 + \frac{12 \ln 2}{\pi^2} \frac{\delta\mu}{T} \right] \quad (\text{S63})$$

The statistical factor is, apparently, linear in excess carrier density:

$$\mathcal{S} = C_{1n}(\alpha_\eta) T \frac{p}{\eta}. \quad (\text{S64})$$

The screening function in this limit is not expressed via elementary functions

$$C_{1n}(\alpha) = \frac{3\alpha^2}{256\pi^4} \int_0^{+\infty} \frac{y^7 dy}{(y^2 + 2\pi\alpha/3)^2} \left[\int_1^{+\infty} \frac{(x^2 - 1) dx}{\text{ch}(y/2) + \text{ch}(xy/2)} \right] \left[\int_{-1}^1 \frac{(1 - x^2) dx}{\text{ch}(y/2) + \text{ch}(xy/2)} \right] \quad (\text{S65})$$

Intra-group recombination. Super-exponential relaxation in the extrinsic node group.

We consider strong pumping of n -doped node of WSM, such that the Fermi levels obey the inequalities

$$T \ll |\mu_v| \ll \mu < \mu_c, \quad (\text{S66})$$

where μ is the Fermi level at equilibrium, and the non-equilibrium value is $\mu_c = \mu + \delta\mu_c$. The pumping is assumed to be strong enough to push the hole quasi-Fermi level into valence band, $\mu_v < 0$.

Again, it is sufficient to model distribution functions as step-wise. The non-equilibrium densities are given by

$$n = \frac{\eta}{2\pi^2} \frac{\mu^2 \delta\mu_c}{v_0^3}, \quad (\text{S67})$$

$$p = \frac{\eta}{6\pi^2} \frac{|\mu_v|^3}{v_0^3}. \quad (\text{S68})$$

The equal excess density condition relates the two quasi-Fermi levels

$$|\mu_v| = \sqrt[3]{3\mu^2 \delta\mu_c} \quad (\text{S69})$$

The dielectric function reads

$$\epsilon(0, q) = 1 + \frac{2\alpha_\eta}{\pi} \frac{\mu^2 + \mu_v^2}{\omega_q^2}. \quad (\text{S70})$$

The statistical factor can be expressed in a closed form

$$\mathcal{S} = C_{2d}(\alpha_\eta) \frac{\mu^2}{\eta^{2/3}} \frac{p^{2/3}}{\eta^{2/3}} + \tilde{C}_{2d}(\alpha_\eta) \mu \frac{p}{\eta}, \quad (\text{S71})$$

where the second term corresponds to the next order of expansion in powers of μ_v/μ . Explicit form of screening functions is

$$C_{2d}(\alpha) = \frac{\alpha^2}{4\pi^{11/3} 6^{1/3}} \left[\left(\alpha + \frac{3\pi}{2} \right) \ln \left(\frac{\pi + 2\alpha}{2\alpha} \right) - \frac{\pi(7\pi + 4\alpha)}{4(\pi + 2\alpha)} \right] \quad (\text{S72})$$

$$C_{2d}(\alpha) \propto -\frac{6^{2/3} \alpha^2 \ln \alpha}{16\pi^{8/3}} \quad (\alpha \rightarrow 0) \quad (\text{S73})$$

$$C_{2d}(\alpha) \rightarrow \frac{6^{2/3}}{144\pi^{2/3}} \quad (\alpha \rightarrow \infty) \quad (\text{S74})$$

$$\tilde{C}_{2d}(\alpha) = \frac{\alpha^2}{12\pi^2} \frac{9\pi^2 + 11\pi\alpha + 6\alpha^2}{(\pi + 2\alpha)^2} - \frac{\alpha^{3/2}(\pi + \alpha)}{(2\pi)^{5/2}} \text{arctg} \left(\sqrt{\frac{\pi}{2\alpha}} \right) \quad (\text{S75})$$

$$\tilde{C}_{2d}(\alpha) \propto -\frac{\alpha^{3/2}}{2^{7/2} \sqrt{\pi}} \quad (\alpha \rightarrow 0) \quad (\text{S76})$$

$$\tilde{C}_{2d}(\alpha) \rightarrow \frac{1}{15} \quad (\alpha \rightarrow \infty) \quad (\text{S77})$$

Intra-group recombination. Exponential relaxation in the extrinsic node group.

At the final stages of relaxation in extrinsic n -doped nodes, both quasi-Fermi levels reside in the conduction band, $\mu_c, \mu_v \gg T > 0$. The distribution function of conduction electrons can be modelled as step-wise, while the valence band distribution function differs from unity by an exponentially small factor:

$$f_v(E) = 1 - \exp\left(\frac{E - \mu_v}{T}\right) \quad (\text{S78})$$

The non-equilibrium carrier densities are

$$n = \frac{\eta}{2\pi^2} \frac{\mu^2 \delta \mu_c}{v_0^3} \quad (\text{S79})$$

$$p \approx \frac{\eta T^2 \delta \mu_v}{v_0^3} e^{-\frac{\mu}{T}}, \quad (\text{S80})$$

while the Fermi levels are linked by equal excess density condition

$$\delta \mu_c \approx \frac{2T^2}{\mu^2} e^{-\frac{\mu}{T}} \delta \mu_v. \quad (\text{S81})$$

When the number of holes is exponentially small, only majority carriers contribute to screening:

$$\epsilon(0, q) = 1 + \frac{2\alpha_\eta}{\pi} \frac{\mu^2}{\omega_q^2} \quad (\text{S82})$$

The statistical factor can be expressed in terms of series over μ/T

$$\mathcal{S} = C_{2n}(\alpha_\eta) \mu \frac{\mu}{T} \frac{p}{\eta} + \tilde{C}_{2n}(\alpha_\eta) \mu \frac{p}{\eta}, \quad (\text{S83})$$

where the screening functions are

$$C_{2n}(\alpha) = \frac{\alpha^2}{12\pi^3} \left[\left(\alpha + \frac{3\pi}{2} \right) \ln \left(\frac{\pi + 2\alpha}{2\alpha} \right) - \frac{\pi(7\pi + 4\alpha)}{4(\pi + 2\alpha)} \right] \quad (\text{S84})$$

$$C_{2n}(\alpha) \propto -\frac{\alpha^2 \ln \alpha}{8\pi^2} \quad (\alpha \rightarrow 0) \quad (\text{S85})$$

$$C_{2n}(\alpha) \rightarrow \frac{1}{72} \quad (\alpha \rightarrow \infty) \quad (\text{S86})$$

, and $\tilde{C}_{2n}(\alpha)$ has a very simple form

$$\tilde{C}_{2n}(\alpha) = \frac{5}{24} \frac{\alpha^2}{(\pi + 2\alpha)^2} \quad (\text{S87})$$

